

Modelling and Simulation of an Autonomous Pod-Tethered Quadcopter Drone System for Aviation Applications

Joshua D'Souza¹, Keith J. Burnham¹, Manolya Kavakli-Thorne² and James E. Pickering¹

¹*School of Engineering and Innovation, Aston University, Birmingham, U.K.*

²*Aston Digital Futures Institute (ADFI), Aston University, Birmingham, U.K.*

Keywords: Drone, Tethered Drone, Control, PID, Autonomous Systems, Safety, Aviation.

Abstract: This paper presents the development of a novel autonomous pod-tethered quadcopter drone system tailored for airport environments. Utilising the Aurrigo Auto-Pod (AAP), the multi-purpose system aims to securely tether a drone that transmits real-time data such as video imagery to the AAP, whilst at the same time supplies power to the drone. Through the development of a novel model-based design (MBD) approach, an analysis of the dynamical behaviour of the tethered system is undertaken. Simulation results demonstrate the potential benefits of using a tethered drone approach to enhance airport operational efficiency and safety. The study highlights the drone's control dynamics and operational constraints within a potential airport setting demonstrating the system's capability to operate under stringent aviation regulations.

1 INTRODUCTION

The research problem addressed in this study centres on developing a novel autonomous pod-tethered quadcopter drone system for airport operation, see Figure 1. It essentially considers the integration of three key components with an Aurrigo Auto-Pod (AAP):

- i. Quadcopter drone
- ii. Tether
- iii. Ground control station

This system must adhere to aviation regulations and cater for the specific operational demands of an airport environment. The objective is to create a prototype tethered drone system that delivers essential information on airport operations, for use onboard the AAP, as depicted in Figure 1. It is envisaged that one function would be that of transmitting video footage from the drone. The onboard control and communication system for the drone is to be securely tethered to the AAP. The tether has the role of not only providing a secure physical link to the AAP, but it also provides a means of transferring data as well as provide a continuous power supply to the quadcopter drone.

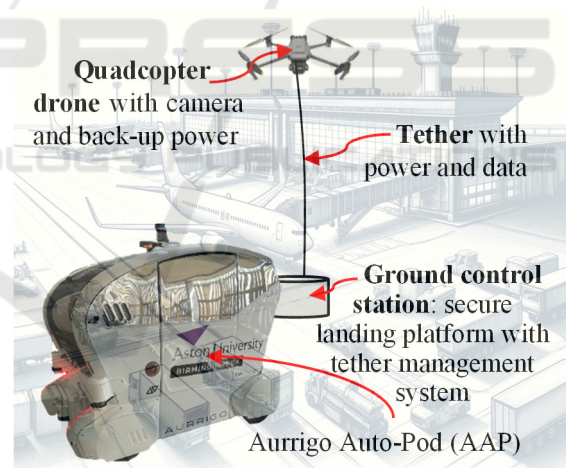


Figure 1: Key operational areas of the autonomous-pod tethered drone system.

In regard to the literature, various tethered drone solutions exist for a range of applications. In (Chang and Hung, 2021), the tethered drone system involves a stationary base station. In (Talke, Birchmore and Bewley, 2022), the tethered drone works with an unmanned surface vehicle (USV) team and operates based on the relative position of the drone and the USV team using data from inertial measurement units (IMUs). In (Kiribayashi, Yakushigawa and Nagatani,

2017), the tethered drone is designed for the operation at disaster sites with a slack tether. In (Kiribayashi, Yakushigawa and Nagatani, 2018), the authors investigated the use of a lightweight tether to reduce the load on the drone; with this being used for drone flights below 10 meters. There is very limited literature on the topic of using autonomous vehicles with tethered drone systems. However, in (Rodrigues, 2023) an approach is proposed and developed for landing a tethered drone on static and moving platforms.

The challenge in this research involves how to effectively 'control' a quadcopter drone that is subject to a tether, which introduces additional complexities to its motion dynamics. Unlike free-flying drones, the tether imposes physical constraints on the drone's range of movement, potentially affecting its stability, maneuverability, and overall performance. The tension in the tether can vary depending on factors such as the drone's velocity, position, and direction, creating nonlinear forces that must be accounted for in the control system. The development of a robust control algorithm that compensates for these tether-induced forces while maintaining smooth, accurate, and responsive flight is key to achieving optimal functionality in tethered drone operations. Additionally, ensuring that the control system can adapt to real-time environmental changes, such as wind or variable tether length, adds another layer of complexity to the problem.

1.1 Aviation Applications of the Tethered Quadcopter Drones

Tethered drones have the potential to be beneficial in a range of airport applications. The tethered drone system satisfies aviation legislation due to the physical connection with the AAP. Applications of tethered drone technology at an airport include:

- Security surveillance: Tethered drones have the potential to offer continuous aerial surveillance of airport premises, enhancing perimeter security by monitoring unauthorised entries, tracking suspicious activities, and deterring potential threats.
- Traffic monitoring and management: Tethered drones can aid in managing ground traffic at large airports by monitoring and optimising the flow of service vehicles, thereby reducing delays, and increasing efficiency.
- Airport inspection: Tethered drones equipped with high-resolution cameras and sensors can potentially facilitate quick and safe inspections of hard-to-reach aircraft parts,

such as the fuselage top and tail, for damage or maintenance issues.

- Emergency response: In emergencies (e.g., fires or accidents on the tarmac), tethered drones can be rapidly deployed to provide real-time video feeds, aiding in accurate situation assessment and effective response coordination.
- Wildlife management: Tethered drones could potentially be used at airports to monitor and manage wildlife activity around runways, preventing bird strikes and enhancing aircraft safety during take-off and landing.
- Weather monitoring: Equipped with meteorological instruments, tethered drones could potentially provide real-time local weather forecast data crucial for managing flight schedules during adverse conditions at airports.
- Construction and maintenance oversight: Tethered drones provide an aerial overview for monitoring progress and ensuring safety protocols during airport construction and maintenance, surpassing ground-based monitoring capabilities.

In this initial piece of research, specific applications such as the points mentioned above will not be explored. Instead, the basic operation of the tethered drone using the AAP will be explored. This basic operation is a starting point for each of the applications outlined above.

1.2 Research Aim and Approach

The aim of the research described in this paper is to develop a novel autonomous pod-tethered drone system tailored specifically to a range of aviation applications and design requirements for these. In this initial study, it will be assumed that the drone will aim to hover at a reference altitude of 10 meters. However, it is envisaged that a further study will be required to explore the optimum altitude for the range of applications. The specific requirements for the tethered drone system have been identified in a series of co-design sessions with the industry partner Aurrigo, see (Pickering, et al, 2024).

To guide and enhance the development of a physical prototype of the autonomous pod-tethered drone system, a model-based design (MBD) approach is adopted. This is used to initially understand the dynamic behaviour of the system and to design and tune the on-board control system. This is because embedded control will be used later when developing the physical prototype. Although initially this would

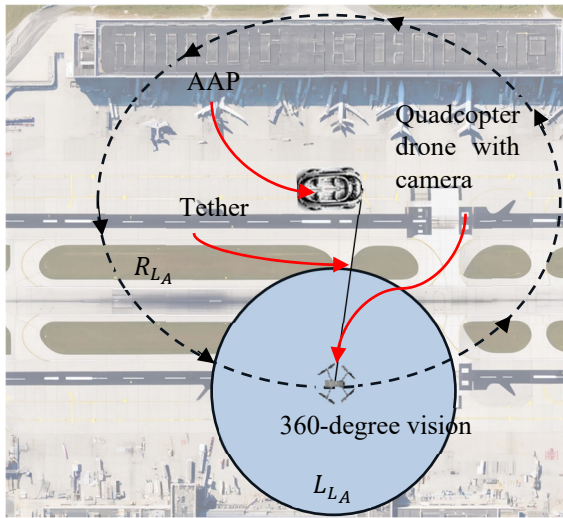


Figure 2: Operation of the autonomous pod-tethered drone system within an airport.

require additional time up-front, it is considered that such an MBD approach over the span of the project will save both time and cost, see (MathWorks, 2020). Figure 2 provides a visualisation of the typical operation of the autonomous pod-tethered drone system at an airport. The MBD approach is used to investigate the potential of the system and to develop the control systems for the following:

- The operation of a tethered drone equipped with a camera that provides the potential for 360-degree vision to scan a local land area, denoted as L_{LA} (in Figure 2, the blue circular area surrounding the drone represents the L_{LA}). In this paper, the actual camera scanning radius is not considered.
- The setup is used to assess the radius of a land area, denoted as R_{LA} , that can be scanned or investigated by a stationary AAP using the tethered quadcopter drone system (in Figure 2, the area within the black dashed line represents the R_{LA} , with the direction of the quadcopter drone motion about the radius provided).

1.3 Outline of Paper

The paper is organised as follows. The novel tethered quadcopter drone simulation model is developed in Section 2. Simulation results are presented and discussed in Section 3. Conclusions of this research and proposals for further work are given in Section 4.

The novelty in the paper is the initial scope of the ideas (i.e., tethered drone with autonomous vehicle)

and the initial mathematical modelling of the tether between the drone and AAP to understand the additional complexities to the drone's motion dynamics.

2 MODELLING AND SIMULATION

A tethered quadcopter drone is to be modelled and simulated to allow the operation of the quadcopter to be explored, i.e., the potential radius of a land area, denoted R_{LA} of the quadcopter drone when tethered. Although beyond the scope of this paper, the developed control systems will then be tested on the actual tethered quadcopter drone system (i.e., physical prototype), using the embedded code tools that are available within MATLAB and Simulink

The key elements of the AAP and tethered system to be developed are the quadcopter drone, and the tether, with the mass of each of the key elements being denoted by m_{AAP} , m_Q , and m_t , respectively. The three masses are subject to gravitational acceleration, denoted g , resulting in a downward force, and drag forces due to the presence of wind disturbances; these are denoted $F_{D_{AAP}}$, F_{D_Q} , and F_{D_t} , respectively, and modelled by:

$$F_{D_{AAP/Q/t}} = \frac{1}{2} \rho A C_D V^2 \quad (1)$$

where ρ is the density of the atmosphere, A is the cross-sectional area perpendicular to the wind flow, C_D is the coefficient of drag, and V is the velocity of the object (White, 2011).

2.1 Quadcopter Dynamics and Control

The schematic in Figure 3 illustrates the quadcopter to be mathematically modelled in this section, with the quadcopter drone presented in three-dimensional space, i.e., X , Y , and Z . The lift generated by the 4 rotors of the quadcopter is denoted U_1 and T denotes the tension acting on a taut line of the tether, denoted t , between the AAP and the quadcopter drone, see Figure 3. Details of the free body diagram for the key elements are also given in Figure 3.

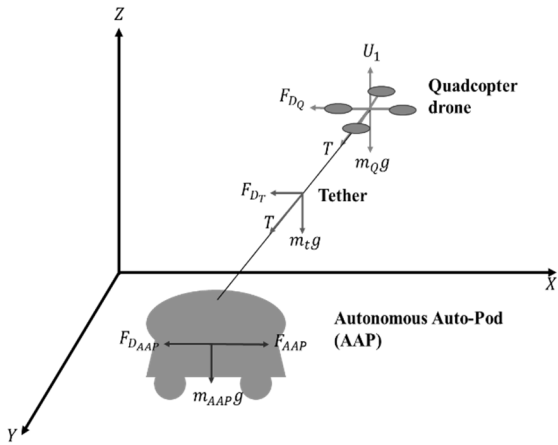


Figure 3: Freebody diagram of the tether system.

The orientation of the quadcopter within the three-dimensional space is defined by the Euler angles, roll, denoted φ , pitch denoted θ and yaw, denoted ψ , see (Abdelhay and Zakriti, 2019). This orientation of the quadcopter drone is defined based on the transformation between the quadcopter drone within the three-dimensional space. This is represented by the following rotational transformation matrix (Abdelhay and Zakriti, 2019):

$$[R] = \begin{bmatrix} c\psi c\theta & s\psi c\theta & -c\psi s\theta & c\psi s\theta c\psi + s\psi s\theta \\ c\theta s\psi & s\theta s\psi & c\psi c\theta & c\psi s\theta s\psi - s\psi c\theta \\ -s\theta & s\psi c\theta & c\psi c\theta & c\psi c\theta \end{bmatrix} \quad (2)$$

where c is the cosine of the Euler angle, s is the sine of the Euler angle, and $[R]$ is the rotational matrix.

In (Abdelhay and Zakriti, 2019), the following equations of motion are used to capture the nonlinear dynamics of the quadcopter:

$$m\ddot{x} = (F_1 + F_2 + F_3 + F_4)(\cos\varphi \sin\theta \cos\psi + \sin\varphi \sin\psi) \quad (3)$$

$$m\ddot{y} = (F_1 + F_2 + F_3 + F_4)(\cos\varphi \sin\theta \cos\psi + \sin\varphi \cos\psi) \quad (4)$$

$$m\ddot{z} = (F_1 + F_2 + F_3 + F_4)(\cos\varphi \cos\theta) - mg \quad (5)$$

$$I_x \ddot{\varphi} = (F_1 - F_3)l + \dot{\theta}\dot{\psi}(I_y - I_z) \quad (6)$$

$$I_y \ddot{\theta} = (F_2 - F_4)l + \dot{\psi}\dot{\varphi}(I_z - I_x) \quad (7)$$

$$I_z \ddot{\psi} = (M_2 + M_4 - M_1 - M_3) + \dot{\varphi}\dot{\theta}(I_x - I_y) \quad (8)$$

where \ddot{x} , \ddot{y} , and \ddot{z} represent the acceleration components. The quadcopter's moments of inertia about the principal axes are given by I_x , I_y , I_z . The moments produced by the rotors are M_1 , M_2 , M_3 and M_4 , and F_1 , F_2 , F_3 and F_4 correspond to the thrust forces generated by each of the quadcopter's rotors.

Based on Equation (3) to (8), the model is linearised (i.e., using small angle approximations, thus eliminating the cosine and sine terms) and rearranged to give the following, see (Ahmad et al., 2020):

$$\ddot{x} = \frac{U_1}{m} \theta \quad (9)$$

$$\ddot{y} = \frac{U_1}{m} \varphi \quad (10)$$

$$\ddot{z} = \frac{U_1}{m} - g \quad (11)$$

$$\ddot{\varphi} = \frac{U_2}{I_x} \quad (12)$$

$$\ddot{\theta} = \frac{U_3}{I_y} \quad (13)$$

$$\ddot{\psi} = \frac{U_4}{I_z} \quad (14)$$

where U_1 , U_2 , U_3 , and U_4 are the control variables that can be further described with the following:

$$U_1 = \sum_{i=1}^4 F_i = K_t \sum_{i=1}^4 \omega_i^2 \quad (15)$$

$$U_2 = (F_1 - F_3)l = K_t l (\omega_1^2 - \omega_3^2) \quad (16)$$

$$U_3 = (F_2 - F_4)l = K_t l (\omega_2^2 - \omega_4^2) \quad (17)$$

$$U_4 = (M_2 + M_4 - M_1 - M_3)l = K_d l (\omega_2^2 + \omega_4^2 - \omega_1^2 - \omega_3^2) \quad (18)$$

where ω_1 , ω_2 , ω_3 , and ω_4 are the angular velocities of the 4 rotors, K_t is the thrust coefficient, K_d is the drag coefficient for the 4 rotors and l signifies the distance from the center of the quadcopter to the center of each rotor.

The initial method of control used for the quadcopter in this research is PID. PID control methods have been widely used for the control of quadcopters, see (Ahmad et al., 2020), (Le Nhu Ngoc Thanh and Hong, 2018), (Zouaoui, Mohamed and Kouider, 2018) and (Xuan-Mung and Hong, (2019), with the control architecture adopted in this research being illustrated in Figure 4. The reference displacements in the x and y axes are given by x_{ref} and y_{ref} , respectively. The PID controllers have been configured and tuned to eliminate steady state error, minimise overshoot and minimise rise time.

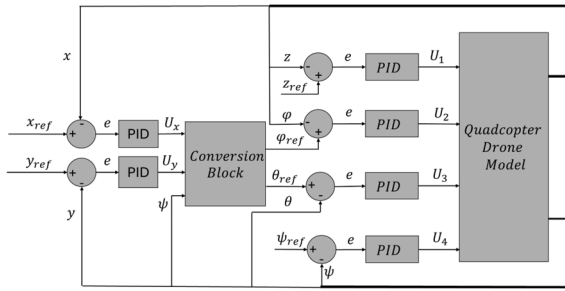


Figure 4: Control architecture of the quadcopter drone, where the bold line indicates multiple signals.

The desired roll and pitch angle references for the drone, denoted φ_{ref} and θ_{ref} , respectively, are determined using the conversion block in Figure 4, which consists of the following:

$$\begin{bmatrix} \varphi_{ref} \\ \theta_{ref} \end{bmatrix} = \begin{bmatrix} \cos\psi & \sin\psi \\ \cos\psi & -\sin\psi \end{bmatrix} \begin{bmatrix} \frac{U_x}{g} \\ \frac{U_y}{g} \end{bmatrix} \quad (19)$$

where use is made of the PID controllers' outputs (i.e., U_x and U_y) for the desired x_{ref} and y_{ref} positions in the three-dimensional space (Ahmad et al., 2020). Note that in further work, PID control is to be compared to other control methods, e.g., LQR and adaptive control.

Regarding the altitude controller, 4 PID controllers are applied to account for the reference/desired altitude, roll angle, pitch angle, and the yaw/heading angle, denoted z_{ref} , φ_{ref} , θ_{ref} and ψ_{ref} , respectively. The controller output accounting for the altitude and the weight of the quadcopter yields the control input, U_1 , which is the collective thrust produced by the 4 rotors. The control inputs, U_2 , U_3 , and U_4 are from the PID controllers which account for roll, pitch, and yaw, respectively.

An initial simulation is configured by considering the parameters in (Abdelhay and Zakriti, 2019). This is initially simulated in order to verify the adopted models, see Figure 5 (a). It is set up such that the initial coordinate location of the quadcopter is (0, 0, 0), with an initial way-point of (1, 0, 10), and then a final coordinate location of (1, 1, 10).

Figure 5 displays the three-dimensional space and trajectory of the quadcopter. Figure 5 also displays the trajectory in each of the respective axes in subplots, i.e., x -axis versus time (b), y -axis versus time (c) and z -axis versus time (d). Displacements in the x and y -axes give a peak overshoot amplitude of 1.004 (i.e., 0.4% overshoot), a 3 second rise time, and 6.5 second settling time. In regard to the displacement in the z -axis, the system response has an amplitude of

10.1 metres. Overall, the quadcopter drone operated as was expected based on results in (Abdelhay and Zakriti, 2019).

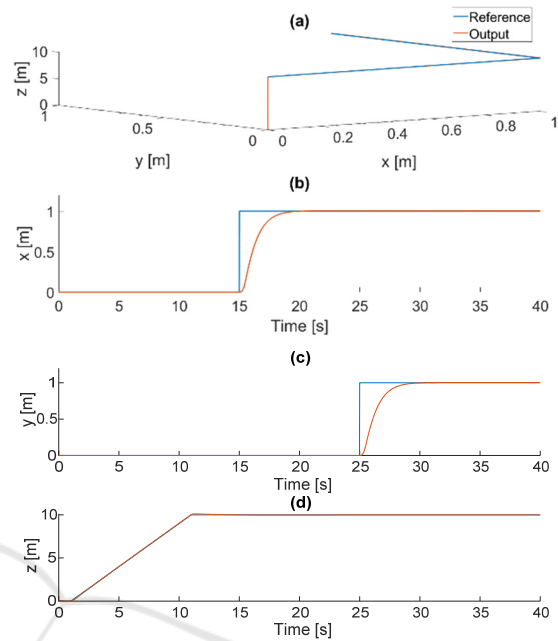


Figure 5: Desired trajectory versus actual trajectory for the quadcopter.

2.2 Tether Dynamics

Tether modelling literature suggests several approaches. One study identifies primary tether forces—drag, weight, and tension—and proposes three configurations: partially-elevated, general fully-elevated, and vertical fully-elevated (Ioppo, 2017). It uses a quasi-static model assuming uniform equilibrium tension, with equations developed for elemental tether lengths under static force balance and specific boundary conditions. Tether dynamics might cause significant tension fluctuations, potentially destabilising the drone, thus it is modelled as a vibrating string with its dynamics defined by wave velocities.

Another study models the tether as rigid-body segments linked at nodes where forces act and position sensors are attached, enabling tether profile recording (Mahmood and Ismail, 2022).

A third study uses the tether for coordinating drones and ground vehicles via force control (Barawkar and Kumar., 2024). Measurable forces and rates through sensors inform a fuzzy-based control system that adjusts drone pitch and yaw. It also includes a PD controller for rotor speed adjustments and an adaptive control for active management under wind conditions.

The physical construction of the novel tether model to be developed here is based on first principles. It is characterised as a cylindrical rod with a uniform circular cross-section of diameter, denoted d_t . The model is further developed with the assumption of being an extendable taut tether throughout the flight operation. Inextensibility is assumed with consideration of a high-modulus, low-elongation material for the tether, which under operational tensile loads exhibits negligible elongation, or stretch. The cylindrical model assumes that the tether's cross-section remains constant despite the wind or aerodynamic forces, which is considered reasonable given the high bending stiffness and the small diameter-to-length ratio.

Consequently, the tether's influence on the quadcopter's dynamics is assumed to be accounted for through static tension and forces that are a function of the tether's material properties, cross-sectional area, and the external environmental loads. The amount of tether required i.e., length, denoted l_t , is dependent of the desired position of the quadcopter with respect to the AAP. The amount of tension on the tether is dependent on the weight of the tether, F_{g_t} and the drag force produced by the wind, $F_{D,t}$. These factors are described by the following:

$$\begin{aligned}
 T &= \begin{bmatrix} T_x \\ T_y \\ T_z \end{bmatrix} = T_0 + F_{g_t} + F_{D_t} \\
 &= \begin{bmatrix} F_{AP_x} - F_{D_{AP_x}} \\ F_{AP_y} - F_{D_{AP_y}} \\ F_{AP_z} - F_{D_{AP_z}} \end{bmatrix} + \begin{bmatrix} 0 \\ 0 \\ \mu l_t g \end{bmatrix} \\
 &+ \begin{bmatrix} F_{D_{t_x}} \\ F_{D_{t_y}} \\ F_{D_{t_z}} \end{bmatrix}
 \end{aligned} \quad (20)$$

where T_x, T_y , and T_z are the tension components in the x, y , and z axes, $F_{D_{AP_x}}, F_{D_{AP_y}}$, and $F_{D_{AP_z}}$ are the drag forces on the AAP, F_{AP_x}, F_{AP_y} , and F_{AP_z} are AAP's driving forces, whilst $F_{D_{t_x}}, F_{D_{t_y}}$, and $F_{D_{t_z}}$ are the drag forces on the tether, and μ is the mass per unit length of the tether.

This section formulates the effects of the dynamics of the quadcopter due to the tether and wind flow. These act as additional loads experienced by the quadcopter, constraining the quadcopter's degrees of freedom. This is due to forces created by tension and wind, and the drag experienced by the quadcopter. These will vary with the quadcopter's position relative to its anchor point. Considering Newton's

second law and Figure 3, the translational motion, from Equations (9) to (11) for the quadcopter and the tether, are now given by:

$$m\ddot{x} = U_1\theta - F_{D_{Q_x}} - T_x \quad (21)$$

$$m\ddot{y} = U_1\varphi - F_{D_{Q_y}} - T_y \quad (22)$$

$$m\ddot{z} = U_1 - mg - F_{D_{Q_z}} - T_z \quad (23)$$

where $F_{D_{Q_x}}, F_{D_{Q_y}}$, and $F_{D_{Q_z}}$ are the drag forces experienced by the quadcopter in the x, y , and z directions, respectively. The drag forces from Equation (1) and modelling in Equation (20) are used and substituted into Equations (21) to (23) to give the following:

$$\ddot{x} = \frac{U_1\theta - \frac{1}{2}\rho_a A_x C_{d_x}(\dot{x} + V_{w_x})^2 - T\cos(\alpha)}{m} \quad (24)$$

$$\ddot{y} = \frac{U_1\varphi - \frac{1}{2}\rho_a A_y C_{d_y}(\dot{y} + V_{w_y})^2 - T\cos(\beta)}{m} \quad (25)$$

$$\ddot{z} = \frac{U_1 - \frac{1}{2}\rho_a A_z C_{d_z}(\dot{z} + V_{w_z})^2 - T\cos(\gamma)}{m - g} \quad (26)$$

where V_{w_x}, V_{w_y} , and V_{w_z} are the wind velocities in the x, y , and z directions, respectively, α, β , and γ are the angles of the tension vector with respect to x, y , and z , respectively, and A_x, A_y , and A_z are reference areas of the quadcopter. In addition to the tether and wind effects on the translation motion of the quadcopter, the generated tension and drag forces introduce constraints in the rotational dynamics of the quadcopter. Hence, Equations (12) to (14) are now given by:

$$\ddot{\phi} = \frac{U_2 - F_{D_x}l_t - T_x d_{CG}}{I_x} \quad (27)$$

$$\ddot{\theta} = \frac{U_3 - F_{D_y}l_t - T_y d_{CG}}{I_y} \quad (28)$$

$$\ddot{\psi} = \frac{U_4 - F_{D_z}l_t - T_z d_{CG}}{I_z} \quad (29)$$

where d_{CG} is the distance between the centre of gravity of the quadcopter and the line of action of the tension force. On this basis, substituting Equations (1) and (21) into Equations (27) to (29) gives the following:

$$\ddot{\phi} = \frac{U_2 - \frac{1}{2} \rho_a A_x C_{a_x} (\dot{x} + V_{w_x})^2 l - T \cos(\alpha) d_{CG}}{I_x} \quad (30)$$

$$\ddot{\theta} = \frac{U_3 - \frac{1}{2} \rho_a A_y C_{a_y} (\dot{y} + V_{w_y})^2 l - T \cos(\beta) d_{CG}}{I_y} \quad (31)$$

$$\ddot{\psi} = \frac{U_4 - \frac{1}{2} \rho_a A_z C_{a_z} (\dot{z} + V_{w_z})^2 l - T \cos(\gamma) d_{CG}}{I_z} \quad (32)$$

where C_{a_x} , C_{a_y} and C_{a_z} are the drag coefficients in the x , y and z -axis, respectively.

3 RESULTS

In this Section, the scenario detailed in Figure 2 will be investigated, i.e., determining the capability of a tethered quadcopter drone system to assess the radius of a land area. For this, the following will be investigated:

- i. Ability of the tethered quadcopter drone to track the radius reference of a land area, denoted as $R_{R_{LA}}$ (see Section I) within a circular path (constant radius) with a varying time-period, denoted T_p .
- ii. Ability of the tethered quadcopter drone to track $R_{R_{LA}}$ with a fixed time-period.
- iii. Ability of the tethered quadcopter drone to track $R_{R_{LA}}$ with a fixed time-period when subject to wind.

3.1 Parameters

Table 1: Tethered quadcopter drone parameters.

Modelling parameter	Value [units]
μ	0.0022 [kg/m]
m	5.2 [kg]
D_t	3.5×10^{-3} [m]
C_{D_t}	0.7
d_{CG}	0.1 [m]
ρ_{air}	1.225 [kg/m ³]
A_x	0.045 [m ²]
A_y	0.045 [m ²]
A_z	0.045 [m ²]
C_D	diag(0.1 0.1 0.15)
C_a	diag(0.1 0.1 0.15)
g	9.81 [m/s ²]
I_x	3.8×10^{-3} [kg/m ²]
I_y	3.8×10^{-3} [kg/m ²]
I_z	7.1×10^{-3} [kg/m ²]
l	0.32 [m]

The parameters used for the simulation studies are given in Tables I and II for the tethered quadcopter drone and the six PID controllers, respectively.

Table 2: PID controller gains for the controlled variables.

Controlled Variable	Controller Gain		
	K_p	K_i	K_d
x	50.00	7.20	30.00
y	11.00	0.16	6.50
z	20.00	5.00	49.96
ϕ	12.00	0.20	7.50
θ	12.00	0.20	7.50
ψ	12.00	0.20	7.50

3.2 Integral of Absolute Errors (IAE) and Data Capture

The integral of absolute error (IAE) is used to evaluate the effectiveness of the controller for the range of scenarios detailed above over a specified interval. This is useful when quantifying the error between a desired control action (i.e., desired position/radius, $R_{R_{LA}}$) and an actual output (i.e., actual position/radius, $O_{R_{LA}}$). The equation for the IAE is given by:

$$IAE = \int_0^T |e(t)| dt \quad (33)$$

where $e(t)$ is the error at time t , which is the difference between the desired output and the actual output, i.e., $e(t) = r(t) - y(t)$, with $r(t)$ being the reference (i.e., desired radius of tethered drone, $R_{R_{LA}}$) and $y(t)$ being the system output (i.e., actual radius of the tethered drone, $O_{R_{LA}}$). T is the time duration over which the error is integrated.

The following simulation results are considered:

- a) First lap (i.e., Lap 1)
- b) 10 laps (not considering Lap 1)

Lap 1 of the simulation is included in the results; this involves the tethered drone system initially transitioning from being transient to steady-state. Note that the initial positioning phase to achieve the desired radius is not included in the IAE result for Lap 1 (this is included only for visual reasons).

For the 10-lap simulation, the graphical outputs and IAE involve capturing Laps 2 to 11 (i.e., 10 laps). As the tethered drone system is in steady state during this period, this is viewed as being a 'better' comparison when comparing IAE for the three investigations detailed above.

3.3 Effect of Time-Period

To investigate the effect of the time period, T_p , a 7-metre radius reference is used for the tethered quadcopter drone.

In Figure 6(a), the tethered drone is initially ‘climbing’ to the reference altitude of 10 metres. The tethered drone then navigates to a reference radius of 7 metres (this is not included in any of the IAE calculations) and proceeds to follow a radius reference of 7 metres.

The full results for the first lap (i.e., Lap 1) and the 10 laps are given in Figure 6 ((a) for Lap 1 and (b) for 10 laps)), with the corresponding IAE results given in Table III. Note that for these results, the IAE is normalised with the time-period. The results indicate that an IAE of 15s represents the ‘best’ results, i.e., lowest error. Time periods of 10s and 20s result in a higher IAE, which would suggest that the quadcopter drone was travelling too fast to achieve the reference (i.e., 10s), or too slow (i.e., 20s).

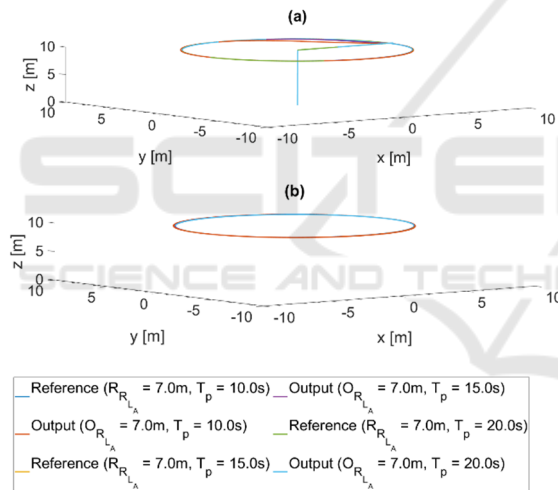


Figure 6: Effect of the time period on achieving the reference.

Table 3: Time period normalised IAE results for Lap 1 and 10 laps.

Time Period [s]	Normalised IAE	
	Lap 1	10 Laps
10.0	0.23	1.05
15.0	0.07	0.01
20.0	0.05	0.03

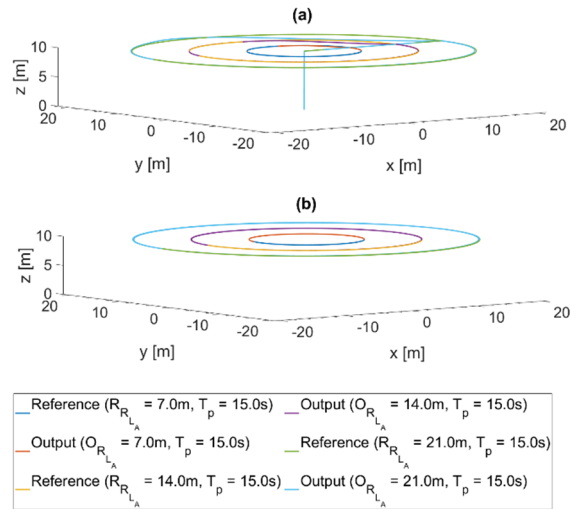


Figure 7: Effect of the radius on achieving the reference.

Table 4: Radius IAE results for Lap 1 and 10 laps.

Radius [m]	IAE	
	Lap 1	(10 Laps)
7	1.00	1.95
15	4.87	5.18
21	13.83	10.13

3.4 Effect of Radius

A set time-period of 15 seconds is selected (as this gave the lowest IAE value in the previous Section), with the tethered quadcopter drone radius reference investigated with values of 7, 15 and 21m.

The full results for the first lap (i.e., Lap 1) and 10 laps are given in Figure 7 ((a) for Lap 1 and (b) for 10 laps)), with the corresponding IAE results given in Table IV. For Lap 1 and 10 laps, as the radius increases, the IAE increases, i.e., reducing the ability of the tethered drone system to follow the circular path.

3.5 Effect of Wind

For this set of results, the radius reference is 7 metres with a time period of 15 seconds. The velocity of the wind in the y-axis, denoted V_{wy} , has been varied with the following values: 5, 10 and 15m/s. In (Choi, 2015), it is highlighted that wind acts as a disturbance, with the wind altering the drone’s altitude and velocity.

The full results for the first lap (i.e., Lap 1) and 10 laps are given in Figure 8 ((a) for Lap 1 and (b) for 10 laps)), with the corresponding IAE results given in Table V.

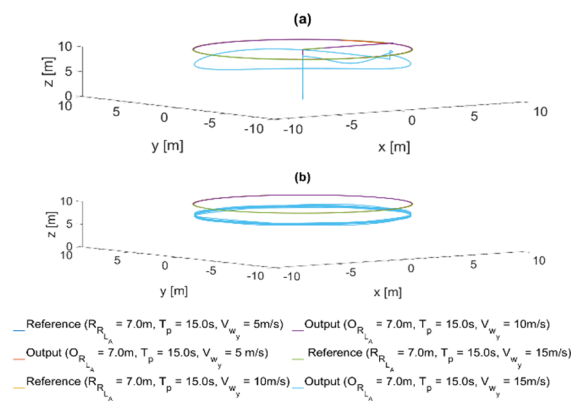


Figure 8: Effect of the wind on achieving the reference.

Table 5: Effects of wind IAE results for Lap 1 and 10 laps.

Wind Velocity in y-axis [m/s]	IAE	
	Lap 1	10 Laps
5	1.02	2.20
10	130	5.51
15	2.06	13.84

For Lap 1 and 10 laps, as the wind speed increases, the IAE increases, with the altitude of the drone decreasing. Thus, the wind reduces the ability of the tethered drone system to achieve the reference altitude. This result is in agreement with the relationship found in (Choi, 2015). It is noticeable that when the wind velocity increases to 15m/s, a large steady state error is introduced for the altitude, i.e., approximately 40%.

4 CONCLUSIONS AND FURTHER WORK

This study has demonstrated the feasibility of a novel autonomous pod-tethered quadcopter drone system, tailored for airport applications, using a novel model-based design (MBD) approach. In particular, the paper has proposed an approach to initially design and tune the control system for a tethered quadcopter drone. The simulation results that have been presented serve to highlight the robustness of the tethered system, under realistic operating conditions, i.e., speed of drone, radius of an operating circle and various wind conditions.

Overall, the results indicate the potential of the system to enhance airport operational efficiency and safety, i.e., offering continuous surveillance, traffic management, as well as rapid emergency response capabilities.

Future work is planned to focus on advancing the modelling and simulation to enhance the overall understanding of the tethered drone's operation. For example, the development of a simulation model to facilitate a comprehensive grasp of the tethered quadcopter's functionality when paired with the Aurrigo Auto-Pod (AAP). Following on from the modeling and simulation, the controller will then be integrated into the physical prototype system of the autonomous pod-tethered quadcopter drone.

ACKNOWLEDGEMENTS

The authors acknowledge the colleagues from Aurrigo, namely James Heaton, Craig Cannon, Nick Ridler and Simon Brewerton for their direction and support with the project.

REFERENCES

Abdelhay, S. and Zakriti, A., 2019. 'Modeling of a quadcopter trajectory tracking system using PID controller', *Procedia Manufacturing*, 32, pp. 564–571. doi:10.1016/j.promfg.2019.02.253.

Ahmad, F., Kumar, P., Bhandari, A. and Patil, P.P., 2020. 'Simulation of the Quadcopter Dynamics with LQR based control', *Materials Today: Proceedings*, 24, pp. 326–332. doi:10.1016/j.matpr.2020.04.282.

Barawkar, S. and Kumar, M., 2024. Active manipulation of a tethered drone using explain-able AI.

Chang, K.H. and Hung, S.K., 2021. Design and implementation of a tether-powered hexacopter for long endurance missions. *Applied Sciences*, 11(24), p.11887.

Choi, H.S. et al., 2015. Dynamics and simulation of the effects of wind on UAVs and airborne wind measurement, transactions of the Japan society for aeronautical and space sciences, 58(4), pp. 187–192. doi:10.2322/tjsass.58.187.

Ioppo, P.G., 2017. *The design, modelling and control of an autonomous tethered multirotor UAV* (Doctoral dissertation, Stellenbosch: Stellenbosch University).

Kiribayashi, S., Yakushigawa, K. and Nagatani, K., 2017, October. Position estimation of tethered micro unmanned aerial vehicle by observing the slack tether. In *2017 IEEE International Symposium on Safety, Security and Rescue Robotics (SSRR)* (pp. 159-165). IEEE.

Kiribayashi, S., Yakushigawa, K. and Nagatani, K., 2018. Design and development of tether-powered multirotor micro unmanned aerial vehicle system for remote-controlled construction machine. In *Field and Service Robotics: Results of the 11th International Conference* (pp. 637-648). Springer International Publishing.

- Kotarski, D., Benic, Z. and Krznar, M., 2016. 'Control design for unmanned aerial vehicles with four rotors', *Interdisciplinary Description of Complex Systems*, 14(2), pp. 236–245. doi:10.7906/indecs.14.2.12.
- Le Nhu Ngoc Thanh, H. and Hong, S.K., 2018. 'Quadcopter robust adaptive second order sliding mode control based on PID sliding surface', *IEEE Access*, 6, pp. 66850–66860. doi:10.1109/access.2018.2877795.
- Liu, C., Ding, L. and Gu, J., 2021. 'Dynamic modeling and motion stability analysis of tethered UAV', *2021 5th International Conference on Robotics and Automation Sciences (ICRAS)* [Preprint]. doi:10.1109/icras52289.2021.9476254.
- Mahmood, K. and Ismail, N.A., 2022. Application of multibody simulation tool for dynamical analysis of tethered aerostat. *Journal of King Saud University-Engineering Sciences*, 34(3), pp.209-216.
- MathWorks, 2020. Model-Based Design for Embedded Control Systems. Available at: model-based-design-with-simulation-white-paper.pdf (mathworks.com) [Assessed 28/03/2024].
- Pickering, J., Ghanami, N., D'Souza, J., Kattayan, S., Kim, J., Burnham, K., Kavakli-Thorne, M., Heaton, J., Cannon, C., Ridler, N., and Brewerton, S. 2024, July. Review, Challenges, System Requirements and Architecture Design for the Operation of a Tethered Drone with an Aurriego Auto-Pod. In *2024 10th International Conference on Control, Decision and Information Technologies (CoDIT)*. IEEE.
- Rodrigues Lima, R., 2023. Exploiting the Advantages and Overcoming the Challenges of the Cable in a Tethered Drone System. PhD thesis.
- Talke, K., Birchmore, F. and Bewley, T., 2022. Autonomous hanging tether management and experimentation for an unmanned air-surface vehicle team. *Journal of Field Robotics*, 39(6), pp.869-887.
- White, F.M., 2011. *Fluid mechanics*. 7th edn. New York: McGraw-Hill Higher Education.
- Xuan-Mung, N. and Hong, S.-K., 2019. 'Improved altitude control algorithm for Quadcopter unmanned aerial vehicles', *Applied Sciences*, 9(10), p. 2122. doi:10.3390/app9102122.
- Zouaoui, S., Mohamed, E. and Kouider, B., 2018. 'Easy tracking of UAV using PID Controller', *Periodica Polytechnica Transportation Engineering*, 47(3), pp. 171–177. doi:10.3311/pptr.10838.